

# Design of a Spatial RPR-2SS Valve Mechanism

**Peter L. Wang**

Robotics and Automation Laboratory,  
University of California,  
Irvine, CA 92697  
e-mail: wangpl1@uci.edu

**Ulrich Rhem**

Dr. Rehm Tunnelling Consultant GmbH,  
Lotzbeckstr., 25, D-77933,  
Lahr 77933, Germany  
e-mail: ru@tunnelling-consultant.de

**J. Michael McCarthy**

Robotics and Automation Laboratory,  
University of California,  
Irvine, CA 92697  
e-mail: jmmccart@uci.edu

*This paper applies kinematic synthesis theory to obtain the dimensions of a constrained spatial serial chain for a valve mechanism that cleans and closes a soil conditioning port in a tunnel boring machine. The goal is a smooth movement that rotates a cylindrical array of studs into position and then translates it forward to clean and close the port. The movement of the valve is defined by six positions of the revolute-prismatic-revolute (RPR) serial chain. These six positions are used to compute the dimensions of the two spherical spherical (SS) dyads that constrain the RPR chain to obtain a one degree-of-freedom spatial mechanism. An example design of this valve mechanism is provided in detail.*  
[DOI: 10.1115/1.4040027]

## 1 Introduction

This paper presents the kinematic synthesis of a spatial mechanism that is proposed for use to clean and close the soil conditioning ports on a tunnel boring machine, Fig. 1. The mechanism combines a rotation and slide of a cylindrical array of studs configured to clean and close the port, when the flow of soil conditioning fluid is stopped. The design process begins with the selection of a spatial revolute-prismatic-revolute (RPR) serial chain that provides the desired rotational and sliding movement. Then two spherical-spherical (SS) linkage are designed to constrain this chain, resulting in an RPR-2SS spatial linkage that moves with one degree-of-freedom, Fig. 2.

The conceptual design of the self-cleaning valve required a system driven by a check valve opening that both cleans the injection port and prevents back flow of soil into the port. An RPR serial chain satisfied these three criteria. The rotation,  $\theta_1$ , of a pressure plate in the soil conditioning line is used to generate two output movements: (i) a slide  $d_2$  of an array of studs that clean the port, and (ii) a rotation  $\theta_3$  that seals the port. This mechanism provides a regular cleaning operation to remove soil build-up from the soil conditioning ports when pressure is relieved during the ring build phase, or during any required down-time, which is a regular part of the tunneling process. Currently, ports are cleaned infrequently when there is a complete blockage. This regular cleaning

operation provided by this mechanism can reduce wear and power consumption in mechanized tunneling [1–4].

## 2 Literature Review

A spatial linkage that coordinates the input angle,  $\theta_1$ , with outputs such as the slide  $d_2$  and rotation  $\theta_3$  is called a function generator [5]. Cervantes-Sanchez et al. [6,7] provide design equations for function generators formed using the single-loop spatial linkages revolute-prismatic-spherical-prismatic-revolute and revolute-revolute-revolute-cylindrical-revolute, and note that  $C$  denotes a cylindrical joint. A general formulation of the design equations for spatial linkages is provided by Chen and Roth [8]; also, see McCarthy and Soh [9].

The control of two outputs for a given input is achieved by a two-loop spatial mechanism, see Sandor et al. [10] and Chiang et al. [11]. Chung [12] designs a two-loop spatial linkage to draw a specified curve. This paper follows the kinematic synthesis methodology introduced by Wang et al. [13], who constrained a spatial RRR serial chain to obtain an RRR-2SS spatial linkage that controls the wing swing and pitch angles for a micro air vehicle. Here, we provide the first design procedure for the RPR-2SS spatial linkage.

## 3 The Spatial Revolute-Prismatic-Revolute Chain

To design the RPR-2SS spatial six-bar linkage, the RPR chain must first be specified by the designer. The Denavit-Hartenberg parameters in Table 1 are shown in Fig. 2, where  $\theta_1, d_2$ , and  $\theta_3$  are joint variables and  $\theta_2, d_1, d_3, \alpha_i, i = 1, 2$ , and  $a_i, i = 1, 2$  are specified by the designer.

As shown previously by Wang et al. [13], let  $L_i, i = 1, 2, 3$  be the coordinate frames. The  $z$ -axis lies along the  $i$ th joint, while the  $x$ -axis lies along the common normal to the next joint axis. The following kinematics equations define the position of these links relative to the ground frame:

$$\begin{aligned} \mathbf{T}_1 &= \mathbf{Z}(\theta_1, d_1) \\ \mathbf{T}_2 &= \mathbf{Z}(\theta_1, d_1)\mathbf{X}(\alpha_1, a_1)\mathbf{Z}(\theta_2, d_2) \\ \mathbf{T}_3 &= \mathbf{Z}(\theta_1, d_1)\mathbf{X}(\alpha_1, a_1)\mathbf{Z}(\theta_2, d_2)\mathbf{X}(\alpha_2, a_2)\mathbf{Z}(\theta_3, d_3) \end{aligned} \quad (1)$$

where  $\mathbf{Z}(\theta_i, d_i)$  and  $\mathbf{X}(\alpha_i, a_i)$  are the  $4 \times 4$  homogeneous transforms

$$\begin{aligned} \mathbf{Z}(\theta_i, d_i) &= \begin{bmatrix} \cos \theta_i & -\sin \theta_i & 0 & 0 \\ \sin \theta_i & \cos \theta_i & 0 & 0 \\ 0 & 0 & 1 & d_i \\ 0 & 0 & 0 & 1 \end{bmatrix} \\ \mathbf{X}(\alpha_i, a_i) &= \begin{bmatrix} 1 & 0 & 0 & a_i \\ 0 & \cos \alpha_i & -\sin \alpha_i & 0 \\ 0 & \sin \alpha_i & \cos \alpha_i & 0 \\ 0 & 0 & 0 & 1 \end{bmatrix}, \quad i = 1, 2, 3 \end{aligned} \quad (2)$$

These kinematics equations are used in the design procedure.

## 4 Spherical Spherical Constraint Synthesis

The joint trajectories  $\theta_1(t)$ ,  $d_2(t)$ , and  $\theta_3(t)$  are prescribed functions of parameter  $t$  that define the movement of the RPR serial chain. To create a one degree-of-freedom system, the RPR chain can be constrained by two SS constraints. The SS dyad BC connects frame  $L_2$  on link AD to the ground frame, and the other SS dyad EF connects frame  $L_3$  on link DE to the ground frame, shown in Fig. 2. The loop OABC is an RPSS four bar linkage, which Chen and Roth [8] show has a maximum number of five relative positions that results in a solution space that is a twentieth-order space curve. See Innocenti [14] and McCarthy and Soh [9] for the SS link design equations.

Contributed by the Mechanisms and Robotics Committee of ASME for publication in the JOURNAL OF MECHANISMS AND ROBOTICS. Manuscript received November 1, 2017; final manuscript received March 23, 2018; published online May 31, 2018. Assoc. Editor: Marc Gouttefarde.

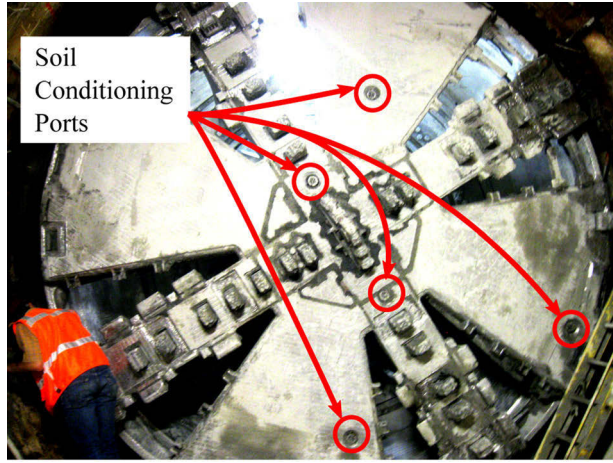


**Fig. 1** Photograph of a tunnel boring machine cutter with arrows identifying the soil conditioning ports

For an SS dyad, the design equations have the linear product decomposition [9]  $\langle x, y, z, 1 \rangle \langle u, v, w, 1 \rangle = 0$ , and has the following expanded form:

$$\langle xu, xv, xw, yu, yv, yw, zu, zv, zw, x, y, z, u, v, w, 1 \rangle \quad (3)$$

However, in the case of constraining an RP serial chain, the polynomial is structured such that  $xw = yw = uz = vz = zw = 0$ . This structure allows for a maximum of six precision points leading to five design equations, leaving a free parameter in the  $z$  direction. To constrain this parameter, an additional constraint equation that contains either  $w, z$ , or both must be added.

To design the one degree-of-freedom system, select six precision points from the three joint trajectories denoted as  $\mathbf{q}_j = (\theta_{1j}, d_{2j}, \theta_{3j}), j = 1, \dots, 6$ .

The configurations of the RPR chain are defined by  $\mathbf{q}_j$ . The moving pivots are measured in ground frame  $F$ . The moving pivots attached to  $L_2$  and  $L_3$  have their coordinates denoted by  $\mathbf{B}^j$  and  $\mathbf{E}^j$ , respectively, for each configuration  $\mathbf{q}_j$ . The relative displacements are introduced

$$\mathbf{R}_{1j} = \mathbf{T}_2(\mathbf{q}_j)\mathbf{T}_2(\mathbf{q}_1)^{-1} \text{ and } \mathbf{S}_{1j} = \mathbf{T}_3(\mathbf{q}_j)\mathbf{T}_3(\mathbf{q}_1)^{-1} \quad (4)$$

which yields

$$\mathbf{B}^j = \mathbf{R}_{1j}\mathbf{B}^1 \text{ and } \mathbf{E}^j = \mathbf{S}_{1j}\mathbf{E}^1 \quad (5)$$

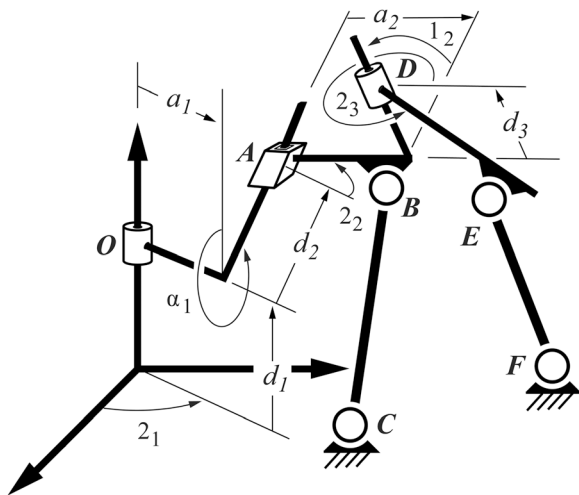


**Fig. 2** The spatial RPR-2SS linkage constructed by constraining a spatial RPR serial chain using two SS dyads that connect the second and third links to the ground frame

**Table 1** Denavit–Hartenberg table for the RPR serial chain.  $\theta_1, d_2$ , and  $\theta_3$  are joint variables. The remaining parameters are selected by the designer.

Link $i$	$\theta_i$	$d_i$	$\alpha_i$	$a_i$
1	$\theta_1$	$d_1$	$\alpha_1$	$a_1$
2	$\theta_2$	$d_2$	$\alpha_2$	$a_2$
3	$\theta_3$	$d_3$	—	—

The SS dyad  $\mathbf{BC}$  has coordinates that must satisfy the constraint equations

$$(\mathbf{R}_{1j}\mathbf{B}^1 - \mathbf{C}) \cdot (\mathbf{R}_{1j}\mathbf{B}^1 - \mathbf{C}) = h^2, \quad j = 1, \dots, 6 \quad (6)$$

where

$$\mathbf{B}^1 = (x, y, z), \quad \mathbf{C} = (u, v, w) \quad (7)$$

Similarly, the SS dyad  $\mathbf{EF}$  has coordinates, which must satisfy

$$(\mathbf{S}_{1j}\mathbf{E}^1 - \mathbf{F}) \cdot (\mathbf{S}_{1j}\mathbf{E}^1 - \mathbf{F}) = k^2, \quad j = 1, \dots, 6 \quad (8)$$

where

$$\mathbf{E}^1 = (m, n, o), \quad \mathbf{F} = (p, q, r) \quad (9)$$

where the lengths of  $\mathbf{BC}$  and  $\mathbf{EF}$  are  $h$  and  $k$ , respectively. Both sets of Eqs. (6) and (8) can be simplified by subtracting the first equation in the set from the remaining five equations. This removes the squared terms for all 12 coordinates of  $\mathbf{BC}$  and  $\mathbf{EF}$  and the constants  $h^2$  and  $k^2$ . The result is the two sets of design equations

$$A_j: (\mathbf{R}_{1j}\mathbf{B}^1 - \mathbf{C}) \cdot (\mathbf{R}_{1j}\mathbf{B}^1 - \mathbf{C}) - (\mathbf{B}^1 - \mathbf{C}) \cdot (\mathbf{B}^1 - \mathbf{C}) = 0 \quad (10)$$

$$j = 2, \dots, 6$$

and

$$B_j: (\mathbf{S}_{1j}\mathbf{E}^1 - \mathbf{F}) \cdot (\mathbf{S}_{1j}\mathbf{E}^1 - \mathbf{F}) - (\mathbf{E}^1 - \mathbf{F}) \cdot (\mathbf{E}^1 - \mathbf{F}) = 0 \quad (11)$$

$$j = 2, \dots, 6$$

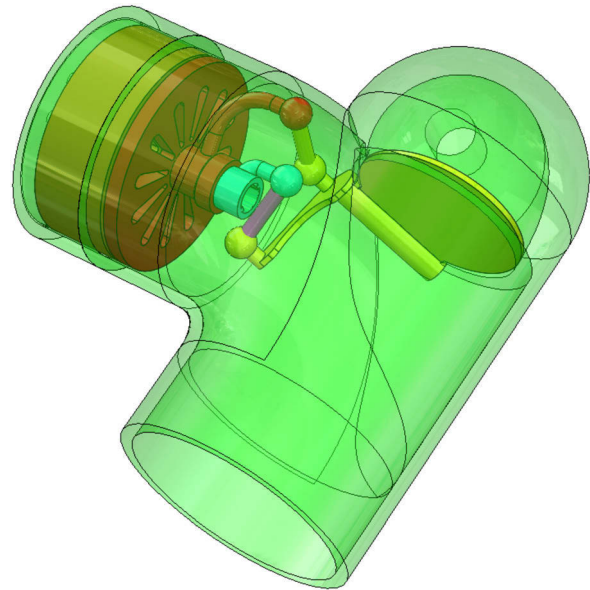


**Fig. 3** The mechanism is mounted inside a T pipe that has one end capped. Flow enters at the bottom left and exits at the top left.

The designer-specified parameter for constraints **BC** and **EF** must be added to the sets of equations  $\mathcal{A}_j$  and  $\mathcal{B}_j$ , respectively. For link **BC**, the free parameter equation must include either  $z$  or  $w$ . There is an additional free parameter for the **EF** constraint that must include either  $o$  or  $r$ . For example, the free parameter equation of link **BC** can be the length of link **OC**, where  $u^2 + v^2 + w^2 = 0$  or to fix joint **B** or **C** to a plane in space, where  $z * x = 0$  or  $w = 0$ , respectively.

The two sets of equations can be solved independently to find pairs of SS dyads that guide the RPR serial chain through six precision points  $\mathbf{q}_j, j = 1, \dots, 6$ . The maximum number of SS dyads depends on chosen free parameter equations.

## 5 Soil Conditioning Valve Mechanism

Our soil conditioning valve mechanism fits within the 4 in diameter pipe that leads to the 3 in diameter port, Fig. 3. This packaging limits the physical dimensions of the RPR spatial chain, which are listed in Table 2. The RPR mechanism uses the prismatic joint to control the plunger, and final revolute joint to control the sealing operation, and the system is actuated by the first revolute joint, Fig. 4. In this figure, fluid flows into the pipe from the bottom left and exits from the top left. Fluid does not flow around the circular pressure plate. The RPR serial chain is to be mounted to the pipe as link  $L_1$ , so the ground link  $F$  is rotated by the fluid pressure within the pipe similar to a swing check valve. Closure of the valve is actuated by a spring when fluid pressure is relieved.

Figure 5 shows the S-joints **C** and **F** are connected to a single crank that drives the slide of link **ABD** and the rotation of link **DE**. The slide of the plunger and the sealing rotations are specified by the designer.

For this design, the trajectory of the slide  $d_2(t)$  was chosen to be a cubic function that provides a decreasing rate of slide relative to the input rotation. The sealing rotation  $\theta_3(t)$  is a linear function that stops when the slide reaches 1.75 in. This allows the plunger to slot into the port closing the valve. These joint trajectories are given by

$$\begin{aligned} \theta_1 &= t \\ d_2 &= -1.25 + 6.37t - 4.56t^2 + 1.16t^3 \\ \theta_3 &= \begin{cases} -\frac{15}{20}t + 0.65 & t < 0.87 \\ 0 & t \geq 0.87 \end{cases} \end{aligned} \quad (12)$$

These functions have been plotted in Fig. 6. The six precision points selected from these trajectories are given in Table 3. The free parameters were chosen such that the joints **C** and **F** are fixed to planes  $w = 0$  and  $r = 0$ , respectively.

The precision points are substituted into the design equations  $\mathcal{A}_j, j = 2, \dots, 6$  for the link **BC**, which results in the following:

$$\begin{aligned} \mathcal{A}_2: & 0.09ux - 0.58uy + 0.21u + 0.58vx + 0.09vy - 0.06v \\ & + 0.22w - 0.22x - 0.22z + 0.023 = 0 \\ \mathcal{A}_3: & 0.34ux - 1.12uy + 0.34u + 1.12vx + 0.34vy - 0.23v \\ & + 0.41w - 0.41x - 0.41z + 0.09 = 0 \\ \mathcal{A}_4: & 0.49ux - 1.31uy + 0.4u + 1.31vx + 0.49vy - 0.35v \\ & + 0.53w - 0.53x - 0.53z + 0.14 = 0 \\ \mathcal{A}_5: & 0.58ux - 1.41uy + 0.49u + 1.41vx + 0.58vy - 0.49v \\ & + 0.69w - 0.69x - 0.69z + 0.24 = 0 \\ \mathcal{A}_6: & 0.97ux - 1.71uy + 0.72u + 1.71vx + 0.97vy - 1.21v \\ & + 1.41w - 1.41x - 1.41z + 0.99 = 0 \end{aligned} \quad (13)$$

From Chen and Roth [8], we find that the RPSS chain can be obtained as the intersection of a fourth order surface with a fifth-

Table 2 Denavit–Hartenberg table for the RPR serial chain

Joint	$\theta_i$	$d_i$	$\alpha_i$	$a_i$
1	$\theta_1$	0.	0.79	1.
2	0.	$d_2$	0.	0.
3	$\theta_3$	1.	—	—

order surface to obtain a 20th order space curve in the moving body. Intersecting the 20th order curve with the hyperplane  $w = 0$  should yield 20 solutions. Based on the design parameters we specified, our solver yielded only five solutions, four complex valued solutions and one real valued solution for  $\mathbf{B}^1 = (x, y, z)$  and  $\mathbf{C} = (u, v, w)$ . The real valued solution is listed in Table 4.

The precision points are substituted into the design equations  $\mathcal{B}_j, j = 2, \dots, 6$  for the link **EF**, which results in the following:

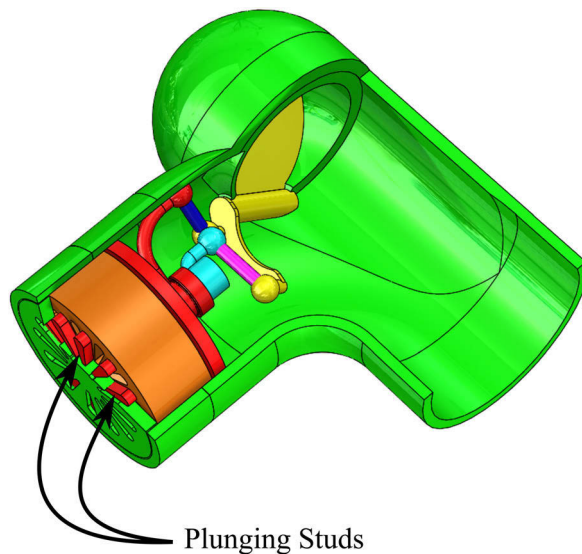


Fig. 4 When the valve closes, it also plunges grate as a self-cleaning action. The studs of the plunger can be seen during the extension phase.

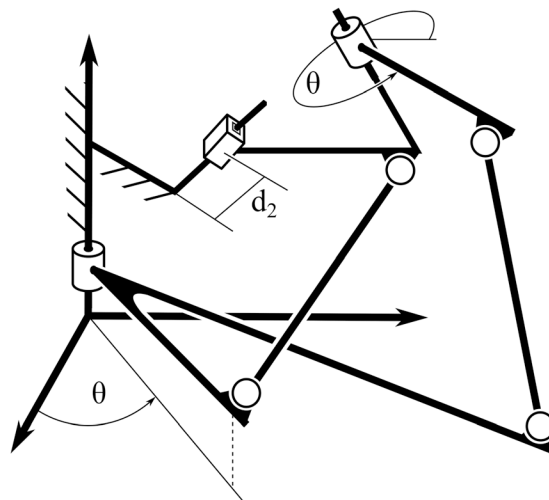
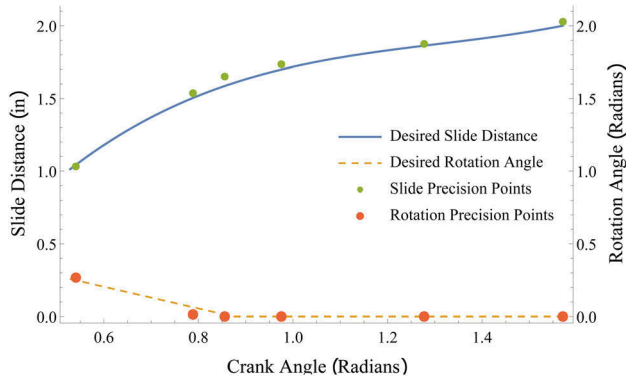


Fig. 5 The link **OA** of the RPR-2SS linkage is held fixed. Points **C** and **F** are connected to a single crank which drive links **ABD** and **DE**.



**Fig. 6 The desired slide and rotation function and the respective precision points are shown. The precision points have been adjusted from the curves during design process.**

$$\begin{aligned}
 B_2: & 0.09mp + 0.58mq - 0.22m - 0.58np + 0.09nq - 0.22o \\
 & + 0.21p - 0.06q + 0.22r + 0.023 = 0 \\
 B_3: & 0.34mp + 1.12mq - 0.41m - 1.12np + 0.34nq - 0.41o \\
 & + 0.34p - 0.23q + 0.41r + 0.086 = 0 \\
 B_4: & 0.49mp + 1.31mq - 0.53m - 1.31np + 0.49nq - 0.53o \\
 & + 0.4p - 0.35q + 0.53r + 0.14 = 0 \\
 B_5: & 0.57mp + 1.4mq - 0.67m - 1.4np + 0.57nq - 0.02nr \\
 & + 0.01op + 0.01oq - 0.71o + 0.48p - 0.48q + 0.71r \\
 & - 2 * 10^{-4}n - 1 * 10^{-4}mr + 1 * 10^{-4}or + .24 = 0 \\
 B_6: & 0.67mp + 1.49mq - 0.04mr - 1.03m - 1.46np \\
 & + 0.69nq - 0.37nr - 0.07n + 0.3op + 0.22oq + 0.04or \\
 & - 1.78o + 0.47p - 0.92q + 1.78r + 1.06 = 0
 \end{aligned} \tag{14}$$

The solution of these equations together with the constraint equation  $r=0$  produce six complex valued solutions and four real valued solution for  $\mathbf{E}^1 = (m, n, o)$  and  $\mathbf{F} = (p, q, r)$ . The real valued solutions are listed in Table 5.

The set of one solution and four solutions combine to create four candidate linkages that are analyzed to verify performance.

## 6 Analysis of RPR-2SS Mechanism

The RPR-2SS mechanism is comprised of two loops: (i) **OABC** forms an RPSS closed chain, (ii) **OADEF** forms an RPRSS closed chain. The determination of the two SS dyads gives the coordinates of  $\mathbf{B}^1\mathbf{C}$  and  $\mathbf{E}^1\mathbf{F}$  and the lengths  $h = |\mathbf{B}^1\mathbf{C}|$  and  $k = |\mathbf{E}^1\mathbf{F}|$ .

**Table 3 Six precision points (radians and inches) of the RPR spatial chain chosen from the joint trajectories to design the SS dyads**

Point $\mathbf{q}_j$	$\theta_1$	$d_2$	$\theta_3$
1	1.57	2.03	0.
2	1.28	1.87	0.
3	0.98	1.73	0.
4	0.86	1.65	0.
5	0.79	1.54	0.01
6	0.54	1.03	0.27

**Table 4 Real-valued solutions to design equations  $\mathcal{A}_j$  for BC**

	$u$	$v$	$w$	$x$	$y$	$z$
1	1.24	1.29	0.00	0.26	0.49	0.30

To determine the movement of the system, first specify the input crank angle  $\theta_1$  then solve the loop constraint equations for  $d_2$  and  $\theta_3$ .

The loop **OABC** has the loop constraint equation

$$(\mathbf{R}_{1q}(\Delta\theta_1, \Delta d_2)\mathbf{B}^1 - \mathbf{C}) \cdot (\mathbf{R}_{1q}(\Delta\theta_1, \Delta d_2)\mathbf{B}^1 - \mathbf{C}) = h^2 \tag{15}$$

where

$$\mathbf{R}_{1q}(\Delta\theta_1, \Delta d_2) = \mathbf{T}_2(\theta_1, d_2)\mathbf{T}_2(\theta_{11}, d_{21})^{-1} \tag{16}$$

and  $\Delta\theta_1 = \theta_1 - \theta_{11}$  and  $\Delta d_2 = d_2 - d_{21}$ .

Expanding this equation yields

$$A(\Delta\theta_1)\Delta d_2^2 + B(\Delta\theta_1)\Delta d_2 + C(\Delta\theta_1) = 0 \tag{17}$$

where the coefficients are listed in Appendix Eq. (A1). The solution to this equation is

$$\Delta d_2 = \frac{-B \pm \sqrt{B^2 - 4AC}}{2A} \tag{18}$$

The loop **OADEF** has the loop constraint equation

$$(\mathbf{S}_{1q}(\Delta\theta_1, \Delta d_2, \Delta\theta_3)\mathbf{E}^1 - \mathbf{F}) \cdot (\mathbf{S}_{1q}(\Delta\theta_1, \Delta d_2, \Delta\theta_3)\mathbf{E}^1 - \mathbf{F}) = k^2 \tag{19}$$

where

$$\mathbf{S}_{1q}(\Delta\theta_1, \Delta d_2, \Delta\theta_3) = \mathbf{T}_3(\theta_1, d_2, \theta_3)\mathbf{T}_3(\theta_{11}, d_{21}, \theta_{31})^{-1} \tag{20}$$

and  $\Delta\theta_3 = \theta_3 - \theta_{31}$ . Expand this equation to obtain

$$D(\Delta\theta_1, \Delta d_2)\cos \Delta\theta_3 + E(\Delta\theta_1, \Delta d_2)\sin \Delta\theta_3 = F(\Delta\theta_1, \Delta d_2) \tag{21}$$

where the coefficients are listed in Appendix Eq. (A2). The solution to this equation is

$$\Delta\theta_3 = \arctan \frac{E}{D} \pm \arccos \frac{F}{\sqrt{D^2 + E^2}} \tag{22}$$

Each value of  $\theta_1$  gives two values for  $d_2$  and two values of  $\theta_3$ , which we label as  $d_2^+, d_2^-$ , and  $\theta_3^+, \theta_3^-$ . The combinations of these values yield four possible joint trajectories

$$\begin{aligned}
 \mathbf{q}^1 &= (\theta_1, d_2^+, \theta_3^+), \mathbf{q}^2 = (\theta_1, d_2^+, \theta_3^-) \\
 \mathbf{q}^3 &= (\theta_1, d_2^-, \theta_3^+), \text{ and } \mathbf{q}^4 = (\theta_1, d_2^-, \theta_3^-)
 \end{aligned} \tag{23}$$

Each of these trajectories represents one branch of the linkage. The selected precision points are compared to the four branches to verify they lie on a single branch. The branch is then checked for continuity between the precision points, which will allow the linkage to smoothly move through all the precision points, thus avoiding branch defects.

## 7 Analysis of the Valve Mechanism

Substitute the coordinates of each of the four combinations of solutions to **BC** and **EF** into Eqs. (18) and (22). From the four candidates, the combinations of solution 1 for **BC** and solutions 2 and 4 for **EF** created linkages that moved smoothly through all the precision points.

**Table 5 Real-valued solutions to design equations  $B_j$  for EF**

	$p$	$q$	$r$	$m$	$n$	$o$
1	3.78	3.41	0.00	0.31	0.56	0.78
2	4.99	-4.04	0.00	-0.14	0.14	5.30
3	1.78	1.53	0.00	0.30	0.49	0.47
4	0.39	-0.02	0.00	-0.33	-0.20	1.00

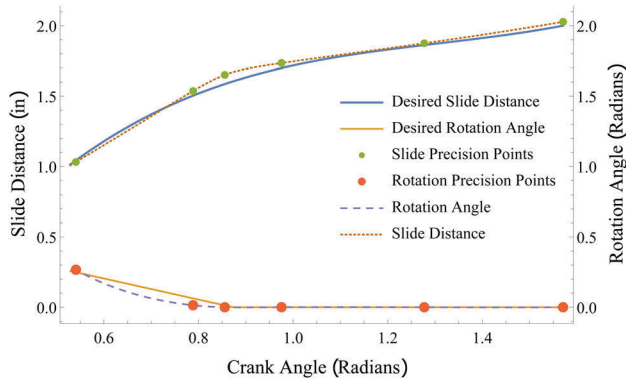


**Fig. 7** The movement of the plunger slide with link BC and sealing rotation with link EF

The selected mechanism combines solution 1 for BC and solution 4 for EF. Solution 2 for EF was eliminated because the link lengths would have been too long to fit in the desired pipe. The performance of the mechanism to control the slide and sealing rotation is compared to the desired curves in Fig. 7 and the selected linkage coordinates are shown in Table 6.

The valve can be seen opening and in the closed position in Figs. 8 and 9. The valve opens when fluid pressurizes the pipe rotating the circular pressure plate. The rotation of the pressure plate drives the slide of the plunger and the sealing rotation.

**Table 6** The links selected for the valve mechanism

BC	$u$	$v$	$w$	$x$	$y$	$z$
	1.24	1.29	0	0.26	0.49	0.30
EF	$p$	$q$	$r$	$m$	$n$	$o$
	0.39	-0.02	0	-0.33	-0.20	1.00

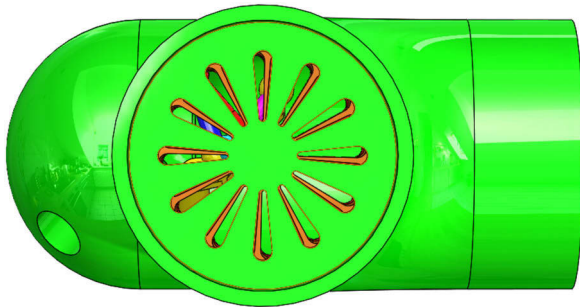


**Fig. 8** The valve is in the process of opening

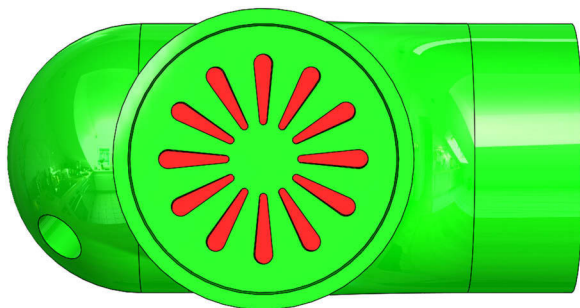


**Fig. 9** The fluid pressure inside of the pipe has decreased below the desired threshold, so the mechanism cleans and seals the port

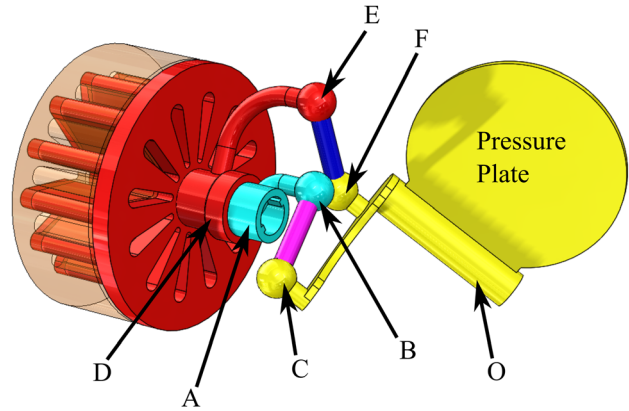


**Fig. 10** This figure shows mechanism with the sealing drum transparent and the pipe hidden. The plunging studs are now visible through the sealing drum.

When fluid pressure decreases, a spring behind the pressure plate will reset the valve to a closed position.

The mechanism can be seen in detail in Fig. 10. The sealing drum is shown to be transparent and the pipe is hidden. Pressure plate is connected to the crank link OCF. The plunger is connected to link ABD. The sealing rotation is controlled by link DE. Link BC connects the crank and the plunger. Link EF, which connects the sealing rotation link to the crank.

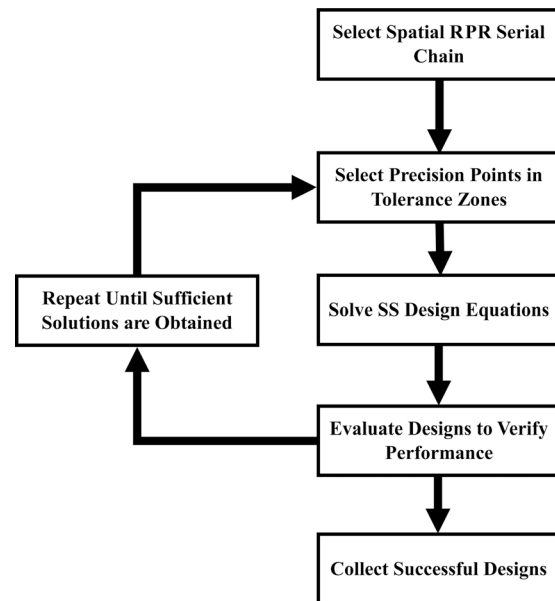


**Fig. 11** The process involves adjustment of the precision points within user defined tolerance zones to find successful designs. Iteration of this procedure produces a large number of design candidates.

**Table 7** The specified tolerance zones from which the precision points are chosen in each iteration

Point $q_j$	$\theta_1$	$d_2$	$\theta_3$
1	1.57	$2.00 \pm 0.05$	0.00
2	$1.31 \pm 0.09$	$1.88 \pm 0.05$	0.00
3	$1.05 \pm 0.09$	$1.75 \pm 0.05$	0.00
4	$0.87 \pm 0.09$	$1.60 \pm 0.05$	0.00
5	$0.79 \pm 0.09$	$1.50 \pm 0.05$	$0.07 \pm 0.09$
6	$0.52 \pm 0.09$	$1.00 \pm 0.05$	$0.26 \pm 0.09$

## 8 Design Process

The design process of soil conditioning valve mechanism follows a similar design process as Wang et al. [13] shown in Fig. 11. First, the designer chooses the functions of the slide and sealing rotation and chooses precision points on those curves within a specified tolerance zone. The design equations for the slide and sealing rotation are solved to find design candidates. The design candidates are then analysed to confirm its performance.

The tolerance zones used are detailed in Table 7. The zones with no allowable deviation were points that the designer could not have deviate. For example, the precision points 1, 2, 3, and 4 for  $\theta_3$  are zero with no allowable deviation are because the mechanism must not rotate while plunging the port. However, the plunging distance and input crank rotation are not as constrained, thus can be varied.

The design process was iterated 2600 times resulting in 459 successful designs. For each iteration, the design equations are solved using new precision points chosen at random within the tolerance zones.

The algorithm was run using Mathematica 10.3 (Champaign, IL) on a workstation with dual 8 core Xeon E5-2620 v4 CPUs running at 2.1 GHz using 16 total threads. The average time of 0.069 s per iteration was found by running the algorithm 11 additional times varying the number of iterations from 2500 to 5200.

The successful designs are sorted in ascending order of the ratio,  $\kappa$ , of the longest to shortest link lengths. Designs with a link length ratio  $\kappa > 10$  were eliminated, leaving 185 designs. The

remaining designs were sorted by the root-mean-square error of the plunge slide and sealing rotations versus their desired movements defined by Eq. (12). Geometric models of the designs are made and animated starting from the designs with the lowest root-mean-square error. The animation allows the designer to determine whether the linkage stays within the desired envelope, the valve body, throughout its movement. The animation also helps the designer determine the feasibility of avoiding interference when physically constructing the linkage. The designer then chooses the mechanism that best fits both the physical constraints and the desired performance.

## 9 Conclusion

This paper presents a mathematical procedure for the design of the RPR-2SS spatial six bar linkage that coordinates a user-defined output slide and output rotation to a specified rotational input. This procedure was demonstrated by designing a valve mechanism to coordinate the plunging and sealing motion of a cylindrical array of studs clean and close a soil conditioning port in a tunnel boring machine. A solid model of the valve is presented, and a prototype is under construction.

## Funding Data

- Division of Civil, Mechanical and Manufacturing Innovation National Science Foundation (Grant No. 1636017).

## Appendix: Coefficients for the Analysis Equations

The coefficients for Eq. (17) are listed here

$$\begin{aligned}
 A(\Delta\theta_1) &= 1 \\
 B(\Delta\theta_1) &= (2d_1 \cos(\alpha_1) - 2u \sin(\alpha_1) \sin(\Delta\theta_1) + 2v \sin(\alpha_1) \cos(\Delta\theta_1) - 2w \cos(\alpha_1) + 2z) \\
 C(\Delta\theta_1) &= (-2a_1 u \cos(\Delta\theta_1) - 2a_1 v \sin(\Delta\theta_1) + 2a_1 x \cos(\theta_2) - 2a_1 y \sin(\theta_2) + a_1^2 - b^2 - 2d_1 w + 2d_1 x \sin(\alpha_1) \sin(\theta_2) \\
 &\quad + 2d_1 y \sin(\alpha_1) \cos(\theta_2) + 2d_1 z \cos(\alpha_1) + d_1^2 + u^2 + 2ux \cos(\alpha_1) \sin(\Delta\theta_1) \sin(\theta_2) - 2ux \cos(\Delta\theta_1) \cos(\theta_2) \\
 &\quad + 2uy \cos(\alpha_1) \sin(\Delta\theta_1) \cos(\theta_2) + 2uy \cos(\Delta\theta_1) \sin(\theta_2) - 2uz \sin(\alpha_1) \sin(\Delta\theta_1) + v^2 - 2vx \cos(\alpha_1) \cos(\Delta\theta_1) \sin(\theta_2) \\
 &\quad - 2vx \sin(\Delta\theta_1) \cos(\theta_2) - 2vy \cos(\alpha_1) \cos(\Delta\theta_1) \cos(\theta_2) + 2vy \sin(\Delta\theta_1) \sin(\theta_2) + 2vz \sin(\alpha_1) \cos(\Delta\theta_1) \\
 &\quad + w^2 - 2wx \sin(\alpha_1) \sin(\theta_2) - 2wy \sin(\alpha_1) \cos(\theta_2) - 2wz \cos(\alpha_1) + x^2 + y^2 + z^2)
 \end{aligned} \tag{A1}$$

The coefficients for Eq. (21) are listed here:

$$\begin{aligned}
 D(\Delta\theta_1) &= (2a_1 m \cos(\theta_2) + 2a_2 m - 2a_1 n \cos(\alpha_2) \sin(\theta_2) + 2d_1 m \sin(\alpha_1) \sin(\theta_2) + 2d_1 n \sin(\alpha_1) \cos(\alpha_2) \cos(\theta_2) \\
 &\quad + 2d_1 n \sin(\alpha_2) \cos(\alpha_1) + 2mp \cos(\alpha_1) \sin(\Delta\theta_1) \sin(\theta_2) - 2mp \cos(\Delta\theta_1) \cos(\theta_2) - 2mq \cos(\alpha_1) \cos(\Delta\theta_1) \sin(\theta_2) \\
 &\quad - 2mq \sin(\Delta\theta_1) \cos(\theta_2) - 2mr \sin(\alpha_1) \sin(\theta_2) + 2\Delta d_2 n \sin(\alpha_2) + 2np \cos(\alpha_1) \cos(\alpha_2) \sin(\Delta\theta_1) \cos(\theta_2) \\
 &\quad + 2np \cos(\alpha_2) \cos(\Delta\theta_1) \sin(\theta_2) - 2np \sin(\alpha_1) \sin(\alpha_2) \sin(\Delta\theta_1) \\
 &\quad - 2nq \cos(\alpha_1) \cos(\alpha_2) \cos(\Delta\theta_1) \cos(\theta_2) + 2nq \cos(\alpha_2) \sin(\Delta\theta_1) \sin(\theta_2) \\
 &\quad + 2nq \sin(\alpha_1) \sin(\alpha_2) \cos(\Delta\theta_1) - 2nr \sin(\alpha_1) \cos(\alpha_2) \cos(\theta_2) - 2nr \sin(\alpha_2) \cos(\alpha_1))
 \end{aligned} \tag{A2}$$

$$\begin{aligned}
 E(\Delta\theta_1) &= (-2a_1 m \cos(\alpha_2) \sin(\theta_2) - 2a_1 n \cos(\theta_2) - 2a_2 n + 2d_1 m \sin(\alpha_1) \cos(\alpha_2) \cos(\theta_2) + 2d_1 m \sin(\alpha_2) \cos(\alpha_1) \\
 &\quad - 2d_1 n \sin(\alpha_1) \sin(\theta_2) + 2\Delta d_2 m \sin(\alpha_2) + 2mp \cos(\alpha_1) \cos(\alpha_2) \sin(\Delta\theta_1) \cos(\theta_2) \\
 &\quad + 2mp \cos(\alpha_2) \cos(\Delta\theta_1) \sin(\theta_2) - 2mp \sin(\alpha_1) \sin(\alpha_2) \sin(\Delta\theta_1) \\
 &\quad - 2mq \cos(\alpha_1) \cos(\alpha_2) \cos(\Delta\theta_1) \cos(\theta_2) + 2mq \cos(\alpha_2) \sin(\Delta\theta_1) \sin(\theta_2) \\
 &\quad + 2mq \sin(\alpha_1) \sin(\alpha_2) \cos(\Delta\theta_1) - 2mr \sin(\alpha_1) \cos(\alpha_2) \cos(\theta_2) \\
 &\quad - 2mr \sin(\alpha_2) \cos(\alpha_1) - 2np \cos(\alpha_1) \sin(\Delta\theta_1) \sin(\theta_2) + 2np \cos(\Delta\theta_1) \cos(\theta_2) + 2nq \cos(\alpha_1) \cos(\Delta\theta_1) \sin(\theta_2) \\
 &\quad + 2nq \sin(\Delta\theta_1) \cos(\theta_2) + 2nr \sin(\alpha_1) \sin(\theta_2))
 \end{aligned}$$

$$\begin{aligned}
F(\Delta\theta_1) = & (2a_2d_1 \sin(\alpha_1)\sin(\theta_2) + 2a_1d_3 \sin(\alpha_2)\sin(\theta_2) + 2 \cos(\alpha_1)(a_2p \sin(\Delta\theta_1)\sin(\theta_2) \\
& + a_2(-q)\cos(\Delta\theta_1)\sin(\theta_2) + d_1\Delta d_2 + \sin(\alpha_2)(d_3 + o)\cos(\theta_2)(q \cos(\Delta\theta_1) - p \sin(\Delta\theta_1)) \\
& + \cos(\alpha_2)(d_3 + o)(d_1 - r) - \Delta d_2r) + 2a_1a_2 \cos(\theta_2) + 2a_1o \sin(\alpha_2)\sin(\theta_2) - 2a_2p \cos(\Delta\theta_1)\cos(\theta_2) \\
& - 2a_1p \cos(\Delta\theta_1) - 2a_2q \sin(\Delta\theta_1)\cos(\theta_2) - 2a_1q \sin(\Delta\theta_1) - 2a_2r \sin(\alpha_1)\sin(\theta_2) + a_1^2 + a_2^2 - b^2 \\
& - 2d_1d_3 \sin(\alpha_1)\sin(\alpha_2)\cos(\theta_2) - 2d_1o \sin(\alpha_1)\sin(\alpha_2)\cos(\theta_2) \\
& + 2 \cos(\alpha_2)(d_3 + o)(\Delta d_2 - p \sin(\alpha_1)\sin(\Delta\theta_1) + q \sin(\alpha_1)\cos(\Delta\theta_1)) + 2d_3o \\
& - 2d_3p \sin(\alpha_2)\cos(\Delta\theta_1)\sin(\theta_2) - 2d_3q \sin(\alpha_2)\sin(\Delta\theta_1)\sin(\theta_2) \\
& + 2d_3r \sin(\alpha_1)\sin(\alpha_2)\cos(\theta_2) - 2d_1r + d_1^2 + d_3^2 + \Delta d_2^2 + m^2 + n^2 + o^2 - 2op \sin(\alpha_2)\cos(\Delta\theta_1)\sin(\theta_2) \\
& - 2oq \sin(\alpha_2)\sin(\Delta\theta_1)\sin(\theta_2) + 2or \sin(\alpha_1)\sin(\alpha_2)\cos(\theta_2) + p^2 \\
& - 2\Delta d_2p \sin(\alpha_1)\sin(\Delta\theta_1) + q^2 + 2\Delta d_2q \sin(\alpha_1)\cos(\Delta\theta_1) + r^2)
\end{aligned}$$

## References

- [1] EFNARC, 2005, *Specification and Guidelines for the Use of Specialist Products for Mechanised Tunnelling (TBM) in Soft Ground and Hard Rock*, EFNARC, Farnham, UK.
- [2] Thewes, M., 1999, "Adhasion Von Tonböden Beim Tunnelvortrieb Mit Flüssigkeitsschilden [Adhesion of Clay Soil During Tunneling With Liquid Shields]," Ph.D. thesis, Universitaet Wuppertal, Wuppertal, Germany.
- [3] Rehm, U., 2004, "Maschinelles Tunnelvortrieb Unter Sehr Schwierigen Geologischen Verhältnissen," Tunnel-Tiefbautagung Gyoer, p. 99.
- [4] Jancsecz, S., Krause, R., Langmaack, L., 1999, "Advantages of Soil Conditioning in Shield Tunnelling: Experiences of Lrts Izmir," *Challenges for the 21st Century*, pp. 865–875.
- [5] Rao, A. M., Sandor, G. N., Kohli, D., and Soni, A., 1973, "Closed Form Synthesis of Spatial Function Generating Mechanism for the Maximum Number of Precision Points," *ASME J. Eng. Ind.*, **95**(3), pp. 725–736.
- [6] Cervantes-Sanchez, J. J., Gracia, L., Alba-Ruiz, E., and Rico, M. J. M., 2011, "Synthesis of a Special Rpspr Spatial Linkage Function Generator for Six Precision Points," *Mech. Mach. Theory*, **46**(2), pp. 83–96.
- [7] Cervantes-Sanchez, J. J., Rico-Martinez, J. M., Perez-Munoz, V. H., and Bitangilgy, A., 2014, "Function Generation With the Rrrcr Spatial Linkage," *Mech. Mach. Theory*, **74**, pp. 58–81.
- [8] Chen, P., and Roth, B., 1969, "Design Equations for Finitely and Infinitesimally Separated Position Synthesis Position Synthesis of Binary Links and Combined Link Chains," *ASME J. Eng. Ind.*, **91**(1), pp. 209–219.
- [9] McCarthy, J. M., and Soh, G. S., 2010, *Geometric Design of Linkages*, Vol. 11, Springer Science & Business Media, New York.
- [10] Sandor, G. N., Xu, L. J., and Yang, S. P., 1986, "Computer-Aided Synthesis of Two-Closed-Loop Rrrs-Ss Spatial Motion Generator Wbranching and Sequence Constraints," *Mech. Mach. Theory*, **21**(4), pp. 345–350.
- [11] Chiang, C. H., Yang, Y.-N., and Chieng, W. H., 1994, "Four-Position Synthesis for Spatial Mechanisms With Two Independent Loops," *Mech. Mach. Theory*, **29**(2), pp. 265–279.
- [12] Chung, W.-Y., 2015, "Synthesis of Spatial Mechanism Ur-2ss for Path Generation," *ASME J. Mech. Rob.*, **7**(4), p. 041009.
- [13] Wang, P. L., Taha, H. E., and McCarthy, J. M., 2018, "Synthesis of a Flapping Wing Mechanism Using a Constrained Spatial Rrr Serial Chain," *ASME J. Mech. Rob.*, **10**(1), p. 011005.
- [14] Innocenti, C., 1995, "Polynomial Solution of the Spatial Burmester Problem," *ASME J. Mech. Des.*, **117**(1), pp. 64–68.